IEEE Access
Multidisciplinary | Rapid Review | Open Access Journal

Received April 10, 2019, accepted April 29, 2019, date of publication May 16, 2019, date of current version June 17, 2019.

Digital Object Identifier 10.1109/ACCESS.2019.2917333

Modeling and Optimization Control for an Engine Electrified Cooling System to Minimize Fuel Consumption

LIANG LU[1,2], HONG CHEN[1,2], (Senior Member, IEEE), YUNFENG HU[1,2], XUN GONG[3], AND ZHIXIN ZHAO[4]

[1]State Key Laboratory of Automotive Simulation and Control, Jilin University, Changchun 130025, China
[2]College of Communication Engineering, Jilin University, Changchun 130025, China
[3]School of Artificial Intelligence, Jilin University, Changchun 130012, China
[4]College of Mathematics, Changchun Normal University, Changchun 130032, China

Corresponding author: Yunfeng Hu (huyf@jlu.edu.cn)

This work was supported in part by the National Natural Science Foundation of China under Grant 61703177, Grant 61773009, and Grant 11601040, in part by the Natural Science Foundation of Jilin Province under Grant 20180101037JC and Grant 20190302119GX, in part by the Funds for Joint Project of Jilin Province and Jilin University under Grant SXGJSF2017-2-1-1, and in part by the Project of Science and Technology Department of Jilin Province under Grant JJKH20180144KJ.

ABSTRACT The engine friction and actuator power are the main factors of the cooling system affecting the fuel economy of a spark ignition (SI) engine. An electrified cooling system containing an electric fan, pump, and thermostat provides an opportunity to reduce fuel consumption. The coolant temperature is always kept at a high fixed value within the safe temperature range to avoid friction losses caused by overcooling; however, the actuator power is not typically considered. Recent publications have attempted to minimize the actuator power and the coolant temperature is maintained in a range. Nevertheless, neither method quantitatively considers both factors. In this paper, the integrated consideration of engine friction and actuator power is presented to minimize engine fuel consumption. The accuracy of a control-oriented model of a cooling system is improved first in an attempt to exert the full potential of the model. Then, the proposed strategy for minimum fuel consumption is constructed as an optimization problem and the improvement of fuel economy obtained by the proposed strategy is evaluated using a causal suboptimal controller and dynamic programming (DP)-based global optimal controller. Compared with a causal coolant temperature tracking controller, the causal suboptimal controller and the global optimal controller based on the proposed strategy both achieve significant improvements. Compared with a global optimal controller for minimum actuator power, the global optimal controller based on the proposed strategy achieves a certain improvement and this effect can increase as the environmental temperature decreases. Finally, a real-time implementation of the proposed strategy on a hardware platform using model predictive control (MPC) with a limited horizon is presented, which shows the feasibility of the proposed strategy.

INDEX TERMS Electrified cooling system, minimum fuel consumption, spark ignition engine, physics-based model, model predictive control (MPC), thermal management system.

I. INTRODUCTION

As is known, most of fuel combustion energy in an engine is wasted by the coolant and exhaust gas, engine thermal management is a path with great potential in fuel saving, where many novel technologies have been born, like organic Rankine cycle [1] and turbo generator [2] to recovery the lost heat, exhaust gas recirculation [3] to reduce the exhaust temperature, electrified cooling system to reduce the loss of friction and actuator power, etc. Especially the electrified cooling system that maintains the engine at the ideal thermal state, can improve not only the fuel economy, but also the emissions, reliability, and durability [4].

Conventional cooling systems feature a mechanical pump and fan, which are coupled to the engine crankshaft with specific or limited transmission ratios, and a wax thermostat

The associate editor coordinating the review of this manuscript and approving it for publication was Xiaosong Hu.

valve, whose position is reliant on the temperature characteristics of the wax. Thus, the engine cannot be precisely maintained at an ideal thermal state. Moreover, a conventional cooling system is always designed for the maximum engine load and worst environmental conditions, which rarely occur, therefore, in most common conditions, the behaviors of the actuators will cause engine overcooling, which leads to more friction losses in the engine and power losses in the actuators [5]–[7].

An electrified engine cooling system equipped with electric actuators enables the on-demand supply of coolant and cooling air, which guarantees a better thermal state of the engine and effectively improves the engine performance [6]. Among the indicators of engine performance, fuel economy is focused on. An electrified engine cooling system improves the fuel economy by reducing the friction resistance of the engine and the power losses of the actuators. The friction resistance of a cold engine is 2.5 times that of a fully warmed engine [8], [9], which can be reduced by shortening the warm-up time and maintaining a higher target coolant temperature [10]–[12]. Choukroun *et al.* [11] applied an electric pump to realize a 50% warm-up time reduction and a 2-3% fuel consumption reduction. Kim *et al.* [12] showed that the fuel consumption at a coolant temperature of 105° C was 3% less than that at a coolant temperature of 85° C and they also applied an electric pump and thermostat to realize a 25% warm-up time reduction. Zhou *et al.* [13] applied an electric pump, a fan, and a thermostat to provide coolant and oil temperature control with a 57% reduction in the actuator power losses. Cortona and Onder [14] applied an electric pump and a thermostat to reduce the actuator power losses by 16% and to effectively reduce the warm-up time. Some of the above studies did not evaluate the fuel consumption, but the fuel consumption certainly decreases. In addition, an electric engine cooling system has a low cost for saving fuel compared to other engine technologies. Fig. 1 shows a comparison of the fuel-saving costs of various technologies, wherein the fuel-saving costs of optimized engine cooling systems and advanced engine cooling systems are only 150 € to 200 € for 1 km/L [15].

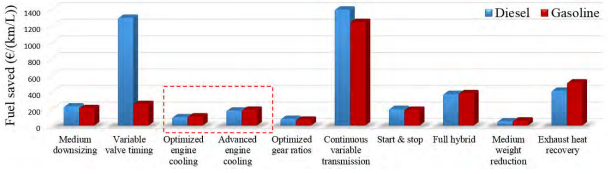

FIGURE 1. Fuel-saving costs of optimized cooling systems and advanced cooling systems compared with those of other various technologies.

Relative studies have addressed the modeling of engine cooling systems, which can be separated into three categories: data-based models, semi-physical models, and physical models. Bruckner *et al.* [16] applied a linear dynamic model and identified the coefficient matrix using steady-state data. Although this modeling method does not necessitate research on the system mechanism, the model accuracy was not guaranteed. Vermillion *et al.* [17] applied the structure of a physical model, but the parameters were identified by steady-state and transient data. This modeling method incorporated transient data, which were hard to collect on an engine test bench. Pizzonia *et al.* [18]–[20] applied a physical model in which only a small amount of steady-state data was necessary, but the model accuracy was very dependent on the understanding of the system.

Studies on the control strategies of electrified cooling systems have mainly concentrated on coolant temperature tracking [11], [20]–[24], which has achieved satisfactory control effects and provided significantly greater engine fuel economy than a traditional cooling system. Fortunately, when the quantity of electric actuators in the cooling system is greater than the number of control objectives, optimization control becomes possible. The optimization control directly correlates the engine performance with the actuator actions that will further improve the engine performance, especially with given knowledge of future driving conditions. Zhou *et al.* [13] designed a causal feedforward and feedback control strategy, where the feedforward minimizes the actuator power under the equality constraint of coolant temperature. The actuator power in their study was 57% less than that in a conventional cooling system, but the contribution to fuel consumption was not evaluated. Nisson *et al.* [25] presented a global optimal controller using dynamic programming (DP) with the knowledge of the entire driving cycle and a causal controller using Pontryagin's minimum principle (PMP) to optimize the actuator power within specified limits of the coolant temperature. By reducing the actuator power, the DP and PMP controllers achieved fuel reductions of 0.31% and 0.28%, respectively, compared with a baseline controller tracking the coolant temperature. However, the paper did not consider the effect of the coolant temperature on the engine friction. Furthermore, both studies did not realize real-time optimization based on future driving conditions.

In this paper, we propose a control strategy for an electrified cooling system to optimize fuel consumption, wherein the actuator power and engine friction are taken into account. To this end, we first develop a dynamic heat transfer model for the cooling system of an SI engine based on the system mechanisms, where two important intermediate variables—heating power from the cylinder to the liner and the cooling power of the radiator—that significantly affect the coolant temperature are focused on. Through the analysis of the heat transfer process, the model accuracies of these two intermediate variables are improved, thereby ensuring the accuracy of the dynamic system model and providing a better optimization solution. Then, the optimization problem for the control strategy of minimum fuel consumption is constructed. A causal controller with unknown future driving conditions is applied to evaluate the effectiveness of the proposed strategy through a comparison with a temperature tracking controller. A DP controller is applied to explore the potential of the proposed strategy with knowledge of an entire driving cycle,

TABLE 1. Nomenclature for main variables.

variable symbol		subscript	
A	Area, m^2	alt	Alternator
C	Heat capacity, J/K	blk	Engine block
H	Valve position	brk	Brake (i.e. effective)
M	Torque, Nm	c	Coolant
N	Rotating speed, r/min	comb	Combustion gas in cylinder
P	Power, W	e	Engine
Q	Heat transfer power, W	ec	Coolant through engine
T	Temperature, K	env	Environment
c_p	Specific heat capacity, J/(kg·K)	f	Fuel
		fan	Fan
h	Convective heat transfer coefficient, J/(m^2·K)	fric	Engine friction
		ind	Indicated
m	Mass flow rate, g/s	lnr	Engine liner
v	Speed, km/h	pump	Pump
		r	Radiator
		ra	Air through radiator
		rc	Coolant through radiator
		th	Thermostat
		vel	Vehicle

and the effectiveness is evaluated compared with the optimization for minimum actuator power. Finally, a real-time model predictive controller (MPC) with a limited horizon is implemented on the hardware platform, which demonstrates the feasibility of the proposed strategy.

The remainder of this paper is organized as follows. In Section II, a mathematical model of the engine cooling system is studied. In Section III, an optimization problem of an electrified cooling system to minimum fuel consumption is formulated. Section IV evaluates the effectiveness of the proposed strategy through comparisons with controllers for coolant temperature tracking and for minimum actuator power. Section V realizes the implementation of the proposed strategy to demonstrate the feasibility of the strategy. Finally, the paper is concluded in Section VI.

II. SYSTEM INTRODUCTION AND MODELING

A. DYNAMIC SYSTEM MODEL

The configuration and heat transfer process of the cooling system in this paper is shown in Fig. 2, wherein the fan, pump, and thermostat are electric actuators. The coolant is circulated between the engine and the radiator by a pump that absorbs heat from the engine and releases heat from the radiator to the environment. The fan promotes the heat release from the radiator. The thermostat is a three-way valve that distributes the coolant flow rate to the inner and outer circuits. When the engine is cold, the thermostat is closed and the radiator is bypassed. When the engine is warm, the thermostat is opened to allow part of the coolant to flow through the radiator. Heat is transferred from the combustion gas in the cylinder to the liner, and then the heat is transferred to the coolant. The coolant removes most of the accumulated heat and the remaining part is transferred to the block and then released to the environment.

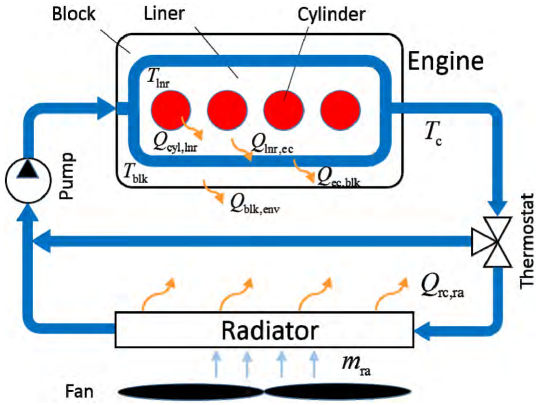

FIGURE 2. Schematic of the configuration and heat transfer process of the cooling system in this paper.

A zero-dimensional cooling system model was developed based on the energy conservation law. The engine liner, block, and coolant temperature are regarded as lumped masses, and the released power from the block to the environment $Q_{\mathrm{blk,env}}$ is ignored. Accordingly, the system behavior is described as follows:

$$C_{\mathrm{lnr}}\dot{T}_{\mathrm{lnr}} = Q_{\mathrm{cyl,lnr}} - h_{\mathrm{e,ec}}(m_{\mathrm{ec}}, T_{\mathrm{c}})A_{\mathrm{lnr,ec}}(T_{\mathrm{lnr}} - T_{\mathrm{c}}), \quad (1a)$$

$$C_{\mathrm{blk}}\dot{T}_{\mathrm{blk}} = h_{\mathrm{e,ec}}(m_{\mathrm{ec}}, T_{\mathrm{c}})A_{\mathrm{blk,ec}}(T_{\mathrm{c}} - T_{\mathrm{blk}}), \quad (1b)$$

$$C_{\mathrm{c}}\dot{T}_{\mathrm{c}} = h_{\mathrm{e,ec}}(m_{\mathrm{ec}}, T_{\mathrm{c}})A_{\mathrm{lnr,ec}}(T_{\mathrm{lnr}} - T_{\mathrm{c}}) - h_{\mathrm{e,ec}}(m_{\mathrm{ec}}, T_{\mathrm{c}})A_{\mathrm{blk,ec}}(T_{\mathrm{c}} - T_{\mathrm{blk}}) - Q_{\mathrm{rc,ra}}, \quad (1c)$$

where C_{lnr}, C_{blk}, and C_{c} are the heat capacities of the liner, block and coolant, respectively, T_{lnr}, T_{blk}, and T_{c} are the temperatures of the liner, block, and coolant, respectively, $Q_{\mathrm{cyl,lnr}}$ is the heating power from the cylinder to the liner, $Q_{\mathrm{rc,ra}}$ is the cooling power of the radiator, $h_{\mathrm{e,ec}}$ is the convective heat transfer coefficient in the water jacket, m_{ec} is the coolant mass flow rate through the engine, $A_{\mathrm{lnr,ec}}$ and $A_{\mathrm{blk,ec}}$ are the heat transfer area.

B. ISSUES WITH THE EXISTING MODELS

Fig. 2 shows that the cylinder and environment are the only heat and cold sources in the cooling system, therefore, the heating power transferred from the cylinder to the liner $Q_{\mathrm{cyl,lnr}}$ and the cooling power of radiator $Q_{\mathrm{rc,ra}}$ significantly affect the coolant temperature. However, the existing models of $Q_{\mathrm{cyl,lnr}}$ and $Q_{\mathrm{rc,ra}}$ have problems pertaining to the unclear expression of the heat transfer mechanism and insufficient analyses of the characteristic variables.

Remark 1: The existing $Q_{\mathrm{cyl,lnr}}$ models include the following expressions.

a) Heywood [28]:

$$Q_{\mathrm{cyl,lnr}} = c \cdot m_{\mathrm{f}}^{n}, \quad (2a)$$

b) Bova *et al.* [29]:

$$Q_{\mathrm{cyl,lnr}} = c \cdot m_{\mathrm{f}}^{n_1} \cdot N_{\mathrm{e}}^{n_2} \cdot m_{\mathrm{ec}}^{n_3}, \quad (2b)$$

c) Zhou *et al.* [13], [14], [19]:

$$Q_{\mathrm{cyl,lnr}} = f(M_{\mathrm{brk}}, N_{\mathrm{e}}), \quad (2c)$$

where m_f is the fuel injection mass flow rate, N_e is the engine speed and M_{brk} is the engine brake torque. The characteristic variables in the expressions above are based only on engineering experience that is not supported by any mechanism analyses of heat transfer processes, therefore, whether these expressions are comprehensive or reasonable is unknown.

Remark 2: The commonly used $Q_{rc,ra}$ model was developed by Cortona *et al.* [14], [19]:

$$Q_{rc,ra} = \alpha_r \cdot A_r \cdot (T_c - T_{env}), \tag{3a}$$

$$\alpha_r \cdot A_r = f(v_{ra}), \tag{3b}$$

where α_r is the radiator heat transfer coefficient, A_r is the radiator heat transfer area, T_{env} is the environment temperature, and v_{ra} is the air flow velocity through the radiator. The Cortona model indicates a large dispersion through validation using data from a GT-Power[1] model, shown in Fig. 3, wherein the sampling points are measured under different air velocities, environmental temperatures, coolant mass flow rates, and coolant temperatures. The large dispersion is caused by an insufficient number of characteristic variables.

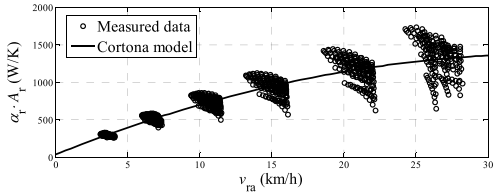

FIGURE 3. Validation results of the Cortona model.

For the above reasons, the models of $Q_{cyl,lnr}$ and $Q_{rc,ra}$ are worth studying. Data used for the study come from a high-fidelity simulation model of an SI engine with an electrified cooling system, which was developed by United Automotive Electronic Systems (UAES).[2] The model is built using GT-Power, which is an industry-standard engine performance simulation software, and the model is calibrated and validated by UAES according to the test data of a certain engine. Except for the engine module, the model also contains transmission system module, vehicle module and road module to link the road conditions to the engine working conditions. The following subsections will present an analysis of the heat transfer process to derive the main characteristic variables and model expressions of $Q_{cyl,lnr}$ and $Q_{rc,ra}$.

C. HEATING POWER FROM THE CYLINDER TO THE LINER

The heat transfer process in the cylinder is complex, involving air flow, fuel evaporation, mixture combustion, and moving pair friction. Previous studies [30], [31] have elaborated the main heat sources to the liner, including combustion, friction, intake flow, and exhaust flow. Moreover, we explored the composition of the heat sources to the liner using a GT-Power

[1]https://www.gtisoft.com/.
[2]http://www.uaes.com/.

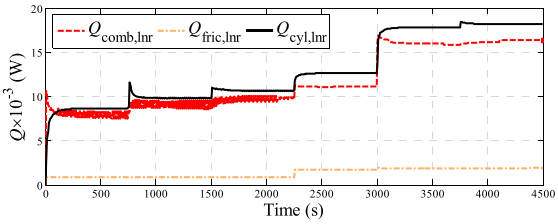

FIGURE 4. Allocation of the heating power from the cylinder to the liner.

model under various working conditions, as shown in Fig. 4, which shows that the ratio of combustion heating power $Q_{comb,lnr}$ and friction heating power $Q_{fric,lnr}$ to $Q_{cyl,lnr}$ is greater than 94% according to the data analysis. Therefore, $Q_{cyl,lnr}$ can be approximated as follows:

$$Q_{cyl,lnr} = Q_{fric,lnr} + Q_{comb,lnr}. \tag{4}$$

The friction between the piston and piston ring is considered boundary friction, which is related to the oil temperature and engine speed. Since the coolant temperature is slightly lower than the oil temperature, $Q_{fric,lnr}$ can be expressed as follows:

$$Q_{fric,lnr} = f(N_e, T_c). \tag{5}$$

The combustion heating power $Q_{comb,lnr}$ involves convective heat transfer and radiative heat transfer between the combustion gas and engine cylinder wall, which can be expressed as follows [32]:

$$Q_{comb,lnr} = h_{comb,lnr}A_{comb,lnr}(T_{comb} - T_{lnr}) + A_{comb,lnr}\kappa[\varepsilon(\frac{T_{comb}}{100})^4 - \zeta(\frac{T_{lnr}}{100})^4], \tag{6}$$

where $h_{comb,lnr}$ is the convective heat transfer coefficient between the combustion gas and cylinder wall, $A_{comb,lnr}$ is the heat transfer area, T_{comb} is the combustion gas temperature, κ is the blackbody radiation coefficient, ε is the combustion gas emissivity and ζ is the cylinder wall absorption ratio. In (6), $h_{comb,lnr}$, T_{comb}, and T_{lnr} are the unknowns that will be studied below.

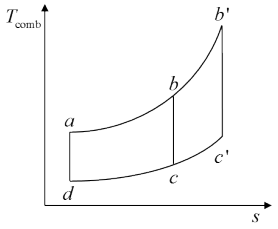

FIGURE 5. The ideal cycle of an SI engine.

The T_{comb}-s curve of the ideal cycle of an SI engine (isothermal heating cycle) is shown in Fig. 5 [33], where s is the specific entropy of the combustion gas. For an engine with a fixed compression ratio, lines c-d, d-a, and a-b are fixed, so only changing the fuel injection per cycle (i.e., the

pressure increase ratio) will change the T_{comb}-s curve, e.g., the increased fuel injection changes the curve from a-b-c-d-a to a-b'-c'-d-a, which increases T_{comb}. In summary, T_{comb} is mainly a function of the fuel injection per cycle, i.e., the fuel injection mass flow rate m_f and engine speed N_e:

$$T_{comb} = f(m_f, N_e). \tag{7}$$

Note that $h_{comb,lnr}$ is approximated as a function of the combustion gas temperature T_{comb} and combustion gas flow velocity in the cylinder v_{comb}, where v_{comb} is related to the intake air and engine speed N_e [34]. For an SI engine, the intake air and the fuel injection amount are a fixed ratio. Therefore, $h_{comb,lnr}$ can be summarized as follows:

$$h_{comb,lnr} = f(m_f, N_e). \tag{8}$$

$Q_{comb,lnr}$ can be obtained by substituting (7) and (8) into (6), and $Q_{cyl,lnr}$ can be obtained by substituting (5) and (6) into (4):

$$Q_{cyl,lnr} = f(m_f, N_e, T_{lnr}), \tag{9}$$

where T_{lnr} cannot be measured in a real engine. By substituting (9) into (1a) and setting $\dot{T}_{lnr} = 0$ in (1a) (T_{lnr} is a slowly changing variable), we obtain the final characteristic variables of $Q_{cyl,lnr}$:

$$Q_{cyl,lnr} = f(m_f, N_e, m_{ec}, T_c). \tag{10}$$

A boundary condition needs to be guaranteed that $Q_{cyl,lnr}$ is zero when m_f is zero. Therefore, according to the trend analysis, the boundary condition and the fitting experience of Bova [29], a high-precision fitting model is summarized as follows:

$$Q_{cyl,lnr} = c \cdot m_f^{n_1} \cdot N_e^{n_2} \cdot m_{ec}^{n_3} \cdot T_c^{n_4}. \tag{11}$$

Each $Q_{cyl,lnr}$ model is compared in Table 2, where the root mean square error (RMSE) and the normalized RMSE[3] (NRMSE) are used as evaluation indexes.

TABLE 2. comparison of the heating power models from the cylinder to the liner.

Model	RMSE	NRMSE
Heywood model (2a)	4102 W	10.4%
Bova model (2b)	1816 W	4.6%
Zhou model (2c)	3592 W	9.1%
Proposed model (11)	1075 W	2.7%

D. COOLING POWER OF THE RADIATOR

The heat power transferred from the coolant to the radiator wall $Q_{rc,r}$ and that from the radiator to the environment $Q_{r.ra}$ are written as follows:

$$Q_{rc,r} = h_{rc,r}(m_{rc}, T_c) \cdot A_r \cdot (T_c - T_r), \tag{12a}$$
$$Q_{r,ra} = h_{r,ra}(m_{ra}, T_{ra}) \cdot A_r \cdot (T_r - T_{ra}), \tag{12b}$$

[3]Percentage of RMSE to the mean of the measured data.

TABLE 3. Comparison of the cooling power models of the radiator.

Model	RMSE	NRMSE
Cortona model (3)	11936 W	23.6%
Proposed model (18)	2704 W	6.4%

where $h_{rc,r}$ and $h_{r,ra}$ are the convective heat transfer coefficients between the coolant and the radiator, and between the radiator and the environment, respectively, m_{rc} and m_{ra} are the coolant and air flow rates through the radiator, respectively, T_{ra} is the air temperature through the radiator and T_r is the temperature of the radiator wall. The dynamic processes of T_r and T_c are analyzed using data from the GT-Power model, when the coolant flow rate and fan speed are varied. The results show that the dynamic process of T_r is less than 5 s, whereas the dynamic process of T_c is approximately 50 s to 500 s. Therefore, it is reasonable to ignore the dynamic process of T_r, i.e. setting $\dot{T}_r = 0$ in (13):

$$C_r \dot{T}_r = Q_{rc,r} - Q_{r,ra}, \tag{13}$$

where C_r is the heat capacity of the radiator, thereby obtaining $Q_{rc,r} = Q_{r,ra}$ (i.e., $Q_{rc,ra}$). According to (12), we get the following expression:

$$T_r = f(m_{rc}, T_c, m_{ra}, T_{ra}), \tag{14}$$

where T_{ra} is unmeasurable, so (14) must be further developed. We approximate T_{ra} as follows:

$$T_{ra} = (T_{ra/out} + T_{env})/2, \tag{15}$$

where $T_{ra/out}$ is the air temperature of the radiator outlet, which can be expressed as (16) according to the heat conservation law:

$$T_{ra/out} = T_{env} + \frac{Q_{rc,ra}}{m_{ra} \cdot c_{pa}}, \tag{16}$$

where c_{pa} is the specific heat capacity of the air. By substituting (16) into (15), and then substituting (14) and (15) into (12b), we get the final characteristic variables of $Q_{rc,ra}$. Therefore, $Q_{rc,ra}$ can be expressed as follows:

$$Q_{rc,ra} = f(m_{rc}, T_c, m_{ra}, T_{env}). \tag{17}$$

The boundary conditions of the model (17) is that when m_{rc} and the temperature difference $T_c - T_{env}$ are zero, $Q_{rc,ra}$ is zero; when m_{ra} is zero, $Q_{rc,ra}$ is not zero since natural convection exists. Then, through the trend analysis of $Q_{rc,ra}$ with each variable, a more reasonable and accurate model of $Q_{rc,ra}$ is derived as (18) and the comparison with the Cortona model is summarized in Table 3.

$$Q_{rc,ra} = c_1 \cdot m_{rc}^{n_1} \cdot (m_{ra}^{n_2} + c_2) \cdot (T_c - T_{env})^{n_3}. \tag{18}$$

The air mass flow rates through the radiator m_{ra} in (18) is calibrated as a map related to the vehicle speed v_{vel} and fan speed N_{fan}:

$$m_{ra} = f_{ra}(N_{fan}, v_{vel}). \tag{19}$$

The coolant mass flow rate through the radiator m_{rc} is:

$$m_{rc} = m_{ec} H_{th}, \tag{20}$$

where $H_{th} \in [0, 1]$ is the thermostat position.

E. SIMPLIFICATION AND VALIDATION OF THE DYNAMIC SYSTEM MODEL

At this point, the dynamic system model has been established in detail. However, the model has three state variables, among which only T_c is considered in the optimization since it has a constraint. Thus, considering the real-time performance of the controller, the dynamic system model needs to be simplified.

Since the state variables change slowly due to the system thermal inertia and have roughly the same trend, $\dot{T}_{lnr}$ and $\dot{T}_{blk}$ are approximately equal to $\dot{T}_c$. Thus, the dynamic system model (1) is simplified as follows:

$$\begin{aligned} C_e \dot{T}_c = {} & Q_{cyl,lnr}(m_f, N_e, m_{ec}, T_c) \\ & - Q_{rc,ra}(m_{rc}(m_{ec}, H_{th}), T_c, m_{ra}(N_{fan}, v_{vel}), T_{env}). \end{aligned} \tag{21}$$

where $C_e = C_{lnr} + C_{blc} + C_c$ is the heat capacity of the engine.

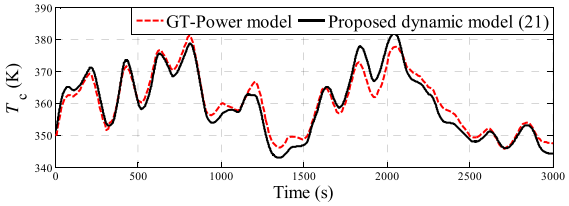

FIGURE 6. Comparison of the high-fidelity GT-Power model and the proposed dynamic model (21).

The simplified dynamic system model (21) is validated using the data from the GT-Power model. Fig. 6 shows a comparison of the coolant temperatures in the GT-Power model and the dynamic system model in response to continuous changes in the engine injection rate, engine speed, coolant flow rate, fan speed, thermostat position, and vehicle speed. The RMSE and NRMSE of the coolant temperature are 2.65 K and 0.73%, respectively.

III. PROBLEM FORMULATION

A. FORMULATION OF THE OBJECTIVE FUNCTION

Given the sequence of required driving conditions, the optimization objective is to find the optimal fan speed, coolant mass flow rate, and thermostat position to minimum the engine fuel consumption, which can be formulated as an optimization control problem in equations, find $u = [N_{fan}\ m_{ec}\ H_{th}]$ such that

$$\min\ J = \int_{t_0}^{t_f} m_f dt, \tag{22}$$

where the fuel consumption rate m_f is expressed as follows:

$$m_f = f_f(M_{ind}, N_e), \tag{23}$$

where f_f denotes the fuel consumption rate, which is represented by a map that is dependent on the engine indicated torque and engine speed.

The engine indicated torque M_{ind} is composed of the engine brake torque M_{brk}, engine friction torque M_{fric} and alternator torque M_{alt}:

$$M_{ind} = M_{brk} + M_{fric} + M_{alt}. \tag{24}$$

Since the engine brake torque M_e and speed N are given as the required driving conditions, the friction torque M_{fric} and alternator torque M_{alt} of the engine are two ways to affect the engine fuel consumption m_f. The models of M_{fric} and M_{alt} are elaborated below.

The engine friction torque M_{fric} is calculated by the following expression:

$$M_{fric} = f_{fric}(M_{brk}, N_e) \cdot f_{corr}(T_c), \tag{25}$$

where f_{fric} denotes the nominal engine friction, which is characterized by a map calibrated at a coolant temperature of 373 K, and f_{corr} is the correction factor, which reflects the impact of the coolant temperature on the engine friction map, as shown in Fig. 7.

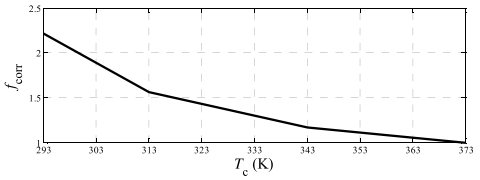

FIGURE 7. Correction factor measuring the impact of the coolant temperature on the engine friction map.

The alternator torque M_{alt} is related to the electrical load. Here, we consider only the actuator power in the cooling system. Therefore, M_{alt} is given by the following expression:

$$M_{alt} = \frac{9550}{\eta \cdot N_e} \cdot (P_{fan} + P_{pump}), \tag{26}$$

where η is the power conversion efficiency from the crankshaft to the actuators. The thermostat power is small in comparison with the fan power and pump power, and is therefore neglected. The fan power is fitted as (27) using data from various fan speeds and vehicle speeds:

$$P_{fan} = c_1 \cdot N_{fan}^3 + c_2 \cdot N_{fan}^2 + c_3 \cdot N_{fan} + c_4, \tag{27}$$

The RMSE and NRMSE of the fan power are 73 W and 6.7%. The pump power is fitted as (28) using data from various coolant flow rates and coolant temperatures:

$$P_{pump} = c_1 \cdot m_{ec}^3 + c_2 \cdot m_{ec}^2 + c_3 \cdot m_{ec} + c_4, \tag{28}$$

The RMSE and NRMSE of the pump power are 5.4 W and 3.9%. The fitting results are shown in Fig. 8.

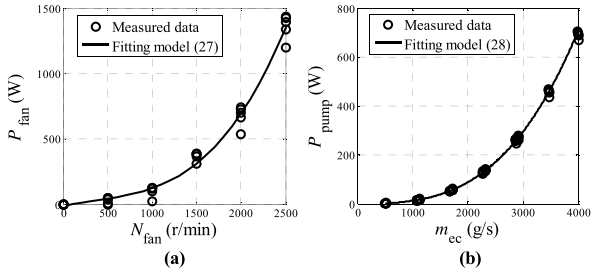

FIGURE 8. Fitting results of the fan power model and the pump power model.

B. OPTIMIZATION PROBLEM STATEMENT

After preparing the dynamic system model and objective function, the optimization problem can be formulated. Substituting the m_f model (23) to (28) into (21), and discretizing the state equation (21) by the Euler method, the following expression can be obtained:

$$x_{k+1} = f(x_k, u_k, w_k), \tag{29}$$

where $u_k = [N_{fan}(k)\ m_{ec}(k)\ H_{th}(k)]'$ are the control variables, $x_k = T_c(k)$ is the state variable, and $w_k = [M_{brk}(k)\ N_e(k)\ v_{vel}(k)\ T_{env}(k)]'$ are the disturbances. The optimization problem is summarized as follows:

$$\min\ J = \sum_{k=1}^{n_p} m_f(u_k, x_k, w_k), \quad k = 1, 2, ..., n_p \tag{30a}$$

which is subject to (29) and

$$x_k < x_{max}, \tag{30b}$$
$$u_k \in U, \tag{30c}$$

where n_p is the predictive step number, x_{max} is the upper limit of the state variable, and U is the set of feasible control variables.

C. OPTIMIZATION PROBLEM SOLUTION

In the offline simulations of Section IV, a causal suboptimal controller and a global optimal controller are necessary to explore the effectiveness of the proposed control strategy. In the causal suboptimal controller, the optimization problem is solved using the ''fmincon'' function in the MATLAB optimization toolbox. In the global optimal controller, the optimization problem is solved using the DP method.

In the real-time implement of Section V, since the ''fmincon'' function is not applicable on the hardware platform and DP cannot compute in real time, the particle swarm optimization (PSO) algorithm is employed to solve the optimization problem. PSO is an iterative method for nonlinear optimization that cannot deal with the state constraint [35]. Thus, we construct a penalty function to transform the state-constrained problem into a state-unconstrained problem. The penalty function is defined as follows:

$$\tilde{J} = \begin{cases} \sum_{k=1}^{n_p} \{e^{\tau \cdot [x_k - x_{max}]} - 1\}, & x_k - x_{max} > 0 \\ 0, & x_k - x_{max} \le 0 \end{cases} \tag{31}$$

where τ is an adjustment parameter. The penalty function increases exponentially when the coolant temperature exceeds the constraint. The optimization problem (30) is improved as follows:

$$\min\ J = \sum_{k=1}^{n_p} m_f(u_k, x_k, w_k) + \tilde{J}, \tag{32}$$

which is subject to (29) and (30c).

IV. EFFECTIVENESS OF THE CONTROL STRATEGY

In this section, three comparisons are carried out to show the effectiveness of proposed control strategy. First (Subsection B) is the comparison of proposed optimization controller for minimum fuel consumption with a temperature tracking controller, where both controllers are causal. The comparison is to explore the fuel consumption improvement of proposed control strategy if there is no driving conditions known. Second (Subsection C) is the comparison of global optimization controller and causal optimization controller, which are both based on the proposed control strategy for minimum fuel consumption. The comparison is to explore the potential of proposed control strategy with prediction. Third (Subsection D) is the comparison of proposed optimization controller for minimum fuel consumption with an optimization controller for minimum actuator power, where both controllers know the entire driving conditions. The comparison is to explore the effect with consideration of engine friction, which is the improvement of proposed control strategy.

A. DRIVING CYCLE

In this paper, the worldwide light-duty test cycle (WLTC) is used to study the effectiveness of the control strategy. The WLTC is classified into three categories according to the power-to-mass ratio (PMR) of a vehicle. This paper selects the Class 3b (PMR > 34) cycle, which is commonly used for passenger cars. The cycle conditions include a low speed phase (0-589 s), a medium speed phase (589-1022 s), a high speed phase (1022-1477 s), and an extra-high speed phase (1477-1800 s), which are characterized by a 131.3 km/h maximum vehicle speed, and more than 50 accelerations and decelerations. Thus, this cycle covers most common driving conditions and can therefore fully verify the effectiveness of the control strategy. The vehicle speed of the WLTC, the required engine torque and engine speed are shown in Fig. 9. It should be noted that the required engine torque and engine speed are extracted from the operation results of the GT-Power model, calculated according to the WLTC profile and vehicle longitudinal dynamics. The self-built vehicle longitudinal dynamics is necessary in practical

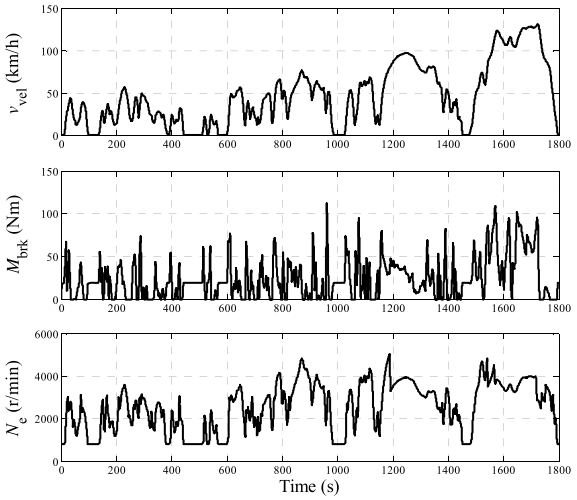

FIGURE 9. Velocity of the WLTC driving cycle and the required engine torque and speed.

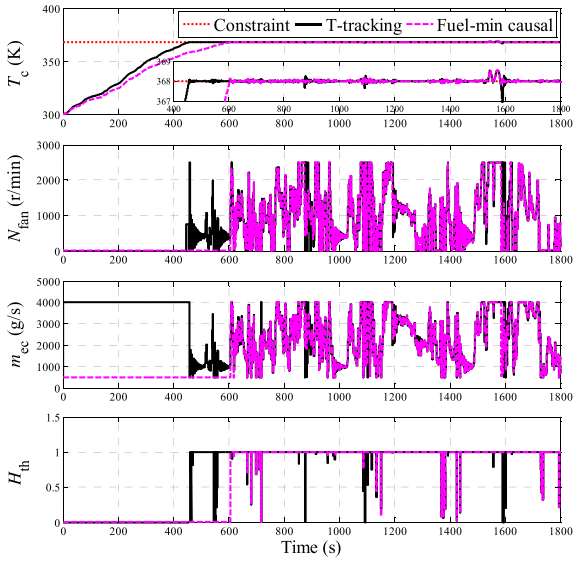

FIGURE 10. Comparison of the coolant temperature tracking controller "T-tracking" and the causal optimization controller "Fuel-min causal" based on the proposed minimum fuel consumption strategy.

application, but it deviates from the main idea of this paper and is not considered here.

B. COMPARISON OF THE CAUSAL OPTIMIZATION CONTROLLER FOR MINIMUM FUEL CONSUMPTION WITH THE TEMPERATURE TRACKING CONTROLLER

In the coolant temperature tracking system, the target temperature is always selected as the upper limit of the allowable value to ensure minimum engine friction. Therefore, in this paper, the upper temperature limit for the optimization controller is also the target temperature for the tracking controller. A coolant temperature tracking controller is used as the baseline controller, which is hereafter referred to as the "T-tracking" controller. The objective of the "T-tracking" controller is to minimize the fuel consumption under the premise of tracking the coolant temperature. The optimization problem of the "T-tracking" controller is the same as (30) with $n_p = 1$, except the state constraint is replaced by $x_k = x_{max}$.

The "T-tracking" controller is a causal controller with unknown future driving conditions. For fair comparison, the proposed control strategy is also set as causal with $n_p = 1$, which we refer to hereafter as the "Fuel-min causal" controller.

TABLE 4. Results of the "t-tracking" controller.

	Warm-up (0-605 s)	Warmed (605-1800 s)	Entire WLTC
Alternator power (kJ)	420.40	757.75	1178.15
Friction power (kJ)	2004.44	7648.55	9652.99
Fuel consumption (g)	347.73	1490.46	1838.19

In both controllers, the discrete time Δt_d and the sampling time Δt are set to 1 s, and the temperature constraint is set to 368 K. The simulation results are shown in Fig. 10. The alternator work, engine friction work, and fuel consumption data are summarized in Tables 4 and 5, wherein the driving cycle

TABLE 5. Results of the "fuel-min causal" controller.

	Warm-up (0-605 s)	Warmed (605-1800 s)	Entire WLTC
Alternator power (kJ)	1.21	703.92	705.13
Friction power (kJ)	2079.71	7648.25	9727.96
Fuel consumption (g)	327.18	1487.29	1814.47

is divided into two phases, for convenient comparison, by the time that the "Fuel-min causal" controller takes to reach the upper temperature limit. The first phase is considered the warm-up phase (0-605 s) and the second phase (605-1800 s) is the warmed phase. Fig. 10 shows that the time required for the "T-tracking" controller and "Fuel-min causal" controller to reach the upper temperature limit is 460 s and 605 s, respectively. The "T-tracking" controller requires less time than the "Fuel-min causal" controller to reach the temperature limit, which is attributed to the maximum coolant flow rate during warm-up. Note that before the thermostat opens, the rise rate of the coolant temperature increases with the coolant flow rate because the increased coolant flow rate leads to increased heating power from the cylinder to the coolant. The higher coolant temperature of the "T-tracking" controller decreases the friction power, whereas the actuator power increases. In the warm-up phase, the friction work of the "T-tracking" controller is less than that of the "Fuel-min causal" controller, whereas the alternator work of the "T-tracking" controller is much greater, therefore, the fuel consumption of the "Fuel-min causal" controller is less than that of the "T-tracking" controller. In the warmed phase, the engine friction is almost the same under both controllers since the coolant temperatures are very close. The alternator work of the "T-tracking" controller is slightly greater than that of the "Fuel-min causal" controller because the equality

constraint of the ''T-tracking'' controller enables more violent actuator action than the unilateral constraint of the ''Fuel-min causal'' controller. Thus, in the warmed phase, the fuel consumption of the ''Fuel-min causal'' controller is slightly less than that of the ''T-tracking'' controller.

In contrast to the ''T-tracking'' controller, the ''Fuel-min causal'' controller significantly reduces the actuator power in the warm-up phase and subsequently reduces the fuel consumption, whereas the ''Fuel-min causal'' controller contributes little to reducing the fuel consumption in the warmed phase.

C. COMPARISON OF THE GLOBAL OPTIMIZATION CONTROLLER WITH THE CAUSAL OPTIMIZATION CONTROLLER

Future driving conditions will undoubtedly further improve the control effect. To explore the potential of the proposed control strategy with entire driving cycle known, the global optimization using DP—referred to hereafter as the ''Fuel-min optimal'' controller—is employed and compared with the ''Fuel-min causal'' controller.

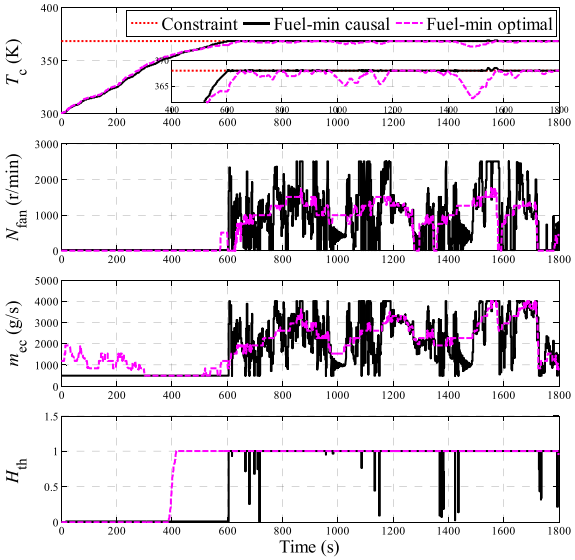

FIGURE 11. Comparison of the causal optimization controller ''Fuel-min causal'' with the global optimization controller ''Fuel-min optimal'', which are both based on the proposed minimum fuel consumption strategy.

In the ''Fuel-min optimal'' controller, the time resolution is 1 s, the coolant temperature resolution is 0.5 K, the fan speed resolution is 250 r/min, the coolant flow rate resolution is 350 g/s, and the thermostat position resolution is 0.1. A comparison of the ''Fuel-min optimal'' controller and the ''Fuel-min causal'' controller is shown in Fig. 11, and the data are summarized in Tables 6 and 7. The separation point between the warm-up and warmed phases is 650 s, which is the time required by the ''Fuel-min optimal'' controller to reach the upper temperature limit. Fig. 11 shows three differences between the ''Fuel-min causal'' and ''Fuel-min optimal'' controllers. 1) Before the thermostat opens, the

TABLE 6. Results of the ''fuel-min causal'' controller.

	Warm-up (0-650 s)	Warmed (650-1800 s)	Entire WLTC
Alternator power (kJ)	26.59	678.54	705.13
Friction power (kJ)	2352.22	7375.74	9727.96
Fuel consumption (g)	377.51	1436.96	1814.47

TABLE 7. Results of the ''fuel-min optimal'' controller.

	Warm-up (0-650 s)	Warmed (650-1800 s)	Entire WLTC
Alternator power (kJ)	15.04	496.39	511.43
Friction power (kJ)	2341.99	7398.27	9740.26
Fuel consumption (g)	377.76	1426.55	1804.31

''Fuel-min causal'' controller maintains the coolant flow at the lower bound, whereas the ''Fuel-min optimal'' controller uses a larger flow rate. This difference occurs because the ''Fuel-min causal'' controller can foresee only one step in the future ($n_p = 1$ in the ''Fuel-min causal'' controller), in which the coolant temperature will hardly change with the present actuator action since it is a slowly changing variable. Therefore, the friction power will hardly decrease with increases in the coolant flow, whereas the actuator power increases, which leads to higher fuel consumption. Therefore, the ''Fuel-min causal'' controller makes an optimal decision for the next step, but not the optimal decision for the entire driving cycle. However, the ''Fuel-min optimal'' controller, which is regarded as possessing a sufficiently long predictive domain, can foresee the coolant temperature variations over the entire driving cycle caused by the present actuator action. Accordingly, the ''Fuel-min optimal'' controller preheats the coolant by increasing the coolant flow to avoid excessive friction power in the future. 2) The ''Fuel-min causal'' controller opens the thermostat until the coolant temperature reaches the upper limit, whereas the ''Fuel-min optimal'' opens the thermostat in advance. The reason for this strategy is that the ''Fuel-min optimal'' can precool the system to avoid excessive actuator power when reaching the upper temperature limit. 3) The coolant temperature of the ''Fuel-min causal'' controller is very close to the upper temperature limit, whereas that of the ''Fuel-min optimal'' controller is well within the upper temperature limit. This finding is also attributed to the precooling of the ''Fuel-min optimal'' controller seeking to avoid excessive actuator power in the future. In addition, the precooling can also prevent the coolant temperature from exceeding the upper limit under heavy engine loads. The results show that at 1550-1600 s, the actuator action of the ''Fuel-min causal'' controller cannot keep the coolant temperature within the limit, whereas the ''Fuel-min optimal'' controller can.

In contrast to the ''Fuel-min causal'' controller, the ''Fuel-min optimal'' controller exploits the knowledge of the entire driving cycle and further reduces the fuel consumption by preheating or precooling, especially in the warmed phase.

D. COMPARISON OF THE GLOBAL OPTIMIZATION CONTROLLER FOR MINIMUM FUEL CONSUMPTION WITH THAT FOR MINIMUM ACTUATOR POWER

To show the advantages of the proposed strategy for minimum fuel consumption, a comparison with a controller for minimum actuator power [25], called the ''Power-min optimal'' controller, is conducted in this paper. The optimization problem for the ''Power-min optimal'' controller is expressed as follows:

$$\min \ J = \sum_{k=1}^{n_p} P_{alt}(N_{fan}(k), m_{ec}(k)), \tag{33}$$

which is subject to (29), (30b), and (30c). Note that the power of the thermostat is always ignored because it is very small.

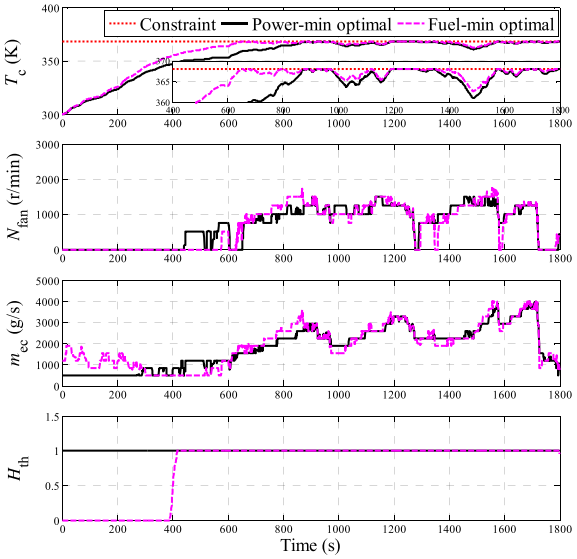

FIGURE 12. Comparison of the optimization controller for minimum actuator power "Power-min optimal" and the optimization controller for minimum fuel consumption "Fuel-min optimal".

TABLE 8. Results of the "power-min optimal" controller.

	Warm-up (0-875 s)	Warmed (875-1800 s)	Entire WLTC
Alternator power (kJ)	70.86	397.84	468.70
Friction power (kJ)	3735.53	6123.46	9858.99
Fuel consumption (g)	608.24	1200.63	1808.87

DP is applied to solve the optimization problem, wherein the resolution settings are the same as those for the ''Fuel-min optimal'' controller stated in Subsection C. The comparison is shown in Fig. 12 and summarized in Tables 7 and 8. The separation point between the warm-up and warmed phases is 875 s, which is the time the ''Power-min optimal'' controller requires to reach the upper temperature limit. Fig. 12 shows two main differences between the ''Power-min optimal'' and ''Fuel-min optimal'' controllers. 1) The thermostat position of the ''Power-min optimal'' controller is maintained at its maximum value, whereas that of the ''Fuel-min optimal'' controller is not. This difference occurs because the thermostat of the ''Power-min optimal'' controller works hard to reduce the coolant temperature to delay the time required to reach the upper temperature limit. This strategy guarantees the smallest actuator power, but at the expense of friction power, and we can see that the coolant temperature rise rate of the ''Power-optimal'' controller is much slower and the friction work in the warm-up phase is much greater. 2) The coolant mass flow of the ''Fuel-min optimal'' controller is initially larger than that of the ''Power-optimal'' controller. The reason for this difference in coolant mass flow is the preheating explained in Subsection C, which helped avoid excessive friction in the future, however, this scenario is not considered by the ''Power-optimal'' controller. Tables 8 and 9 show that the actuator power of the ''Fuel-min optimal'' controller is slightly higher than that of the ''Power-min optimal'' controller, whereas the friction power of the former is lower, especially in the warm-up phase. This finding indicates that the ''Fuel-min optimal'' controller makes compromises between the friction power and actuator power, while the ''Power-optimal'' controller wastes a large amount of friction power in order to achieve lower actuator power. Especially in lower environmental temperatures where the friction is higher, the advantages of the ''Fuel-min optimal'' controller are more obvious, as shown in Fig. 13, in which the fuel consumption saving of the ''Fuel-optimal'' controller is compared with that of the ''Power-optimal'' at various environmental temperatures.

TABLE 9. Results of the "fuel-min optimal" controller.

	Warm-up (0-875 s)	Warmed (875-1800 s)	Entire WLTC
Alternator power (kJ)	105.52	405.91	511.43
Friction power (kJ)	3631.14	6109.12	9740.26
Fuel consumption (g)	604.08	1200.23	1804.31

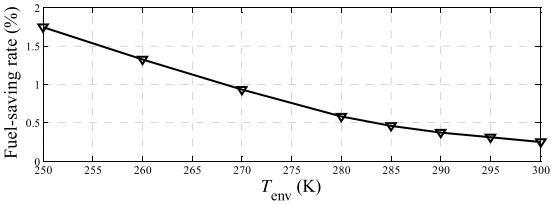

FIGURE 13. Fuel-saving rates of the "Fuel-min optimal" controller compared with those of the "Power-min optimal" controller at various environmental temperatures under the WLTC.

In addition, in the optimization problem (33), the objective function P_{alt} is not dependent on either the thermostat position H_{th} (control variable) or the coolant temperature T_c (state variable), which means that the thermostat position impacts the optimization objective only through the coolant temperature constraint (30b). Therefore, if the predictive coolant temperature cannot reach the constraint in the prediction horizon, the thermostat position will have no effect on the optimization objective, which causes an uncertain solution of the thermostat position H_{th}. The proposed strategy (30) in this paper selects fuel consumption as the optimization objective,

which is related to the thermostat position H_{th} by considering the engine friction, thereby avoiding the uncertain solution of the thermostat position H_{th}.

In contrast to the ''Power-min optimal'' controller, the ''Fuel-min optimal'' controller makes compromises between the friction power and actuator power to realize the minimum fuel consumption, and the fuel saving effects of the ''Fuel-min optimal'' controller are more obvious in lower environmental temperatures. Moreover, the ''Fuel-min optimal'' controller avoids the uncertain solution of the optimization problem of the ''Power-min optimal'' controller.

TABLE 10. Fuel consumption of each controller under various driving cycles.

	T-tracking (g)	Fuel-min causal (g)	Power-min optimal (g)	Fuel-min optimal (g)
WLTC	1838.19	1814.47	1808.87	1804.31
NEDC	952.25	925.99	927.47	923.20
UDDS	1018.69	1003.38	999.52	995.55
FTP75	1015.45	997.31	998.71	994.61
RW	962.20	937.23	933.50	929.94

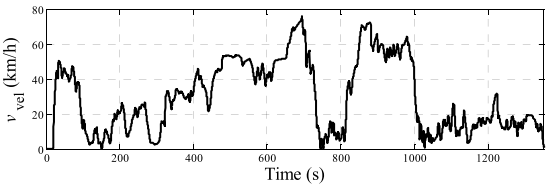

FIGURE 14. Velocity of the real world driving cycle in Changchun, China.

E. SUMMARY OF THE FUEL CONSUMPTION PERFORMANCE OF EACH CONTROLLER

The fuel consumption of each controller under various common driving cycles is summarized in Table 10, including the WLTC, the New European Driving Cycle (NEDC), the Urban Dynamometer Driving Schedule (UDDS), the Federal Test Procedure (FTP75), and a real world (RW) driving cycle. The RW driving cycle is recorded in the urban area of Changchun, China and the velocity of the RW driving cycle is shown in Fig. 14. The required engine torque and engine speed of each driving cycle are extracted from the operation results of the GT-Power model according to the velocity of the corresponding driving cycle. The environmental temperature of the GT-Power model is set as 300 K. Compared with the ''T-tracking'' controller, the ''Fuel-min causal'' controller based on the proposed control strategy without known driving conditions achieves a significant effect that 1.29%-2.76% fuel is saved. Compared with the ''Power-min optimal'' controller, the ''Fuel-min optimal'' controller based on the proposed control strategy with knowledge of entire driving conditions achieves a certain effect that 0.25%-0.46% fuel is saved. Although the improvement is not significant, it is more obvious as the environmental temperature decreases. Moreover, this improvement has almost no cost that only the map of correction factor f_{corr} is to be made. Compared with the ''Fuel-min causal'' controller, the ''Fuel-min optimal'' controller achieves 0.27%-0.78% fuel reduction, which indicates the potential of prediction in the proposed control strategy.

V. REAL-TIME IMPLEMENTATION OF THE CONTROL STRATEGY

From the above study, considering the driving conditions can further improve the fuel consumption. Although the controller in the DP method has an apparent effect, it is actually an offline method that does not consider external disturbances or time consumption. In addition, the behaviors of the cooling system are designed under given driving conditions, which means once the conditions are changed, the effect may be influenced. For the above reasons, an attempt is made to realize the application of the proposed control strategy using a PSO-MPC controller. A dSPACE 1106 is used as the real-time implementation platform.

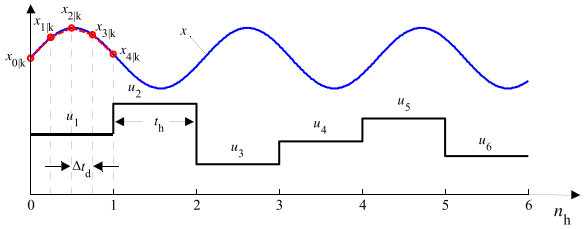

FIGURE 15. Diagram of the MPC framework used in this paper.

Compromising between the computation time and the control effect, the MPC framework used in this paper is shown in Fig. 15, wherein we set the prediction horizon n_h to 6, the horizon length t_h is 20 s, and the discretization interval Δt_d is 5 s, which means the predictive step number is $n_p = 24$ ($n_p = n_h \cdot t_h / \Delta t_d$). The control variables are invariant in each predictive horizon, as shown hereafter:

$$\begin{aligned} u_{1|k} = u_{2|k} = \ldots = u_{(t_h/\Delta t_d)|k} &\triangleq u_1, \\ u_{(t_h/\Delta t_d+1)|k} = u_{(t_h/\Delta t_d+2)|k} &= \ldots = u_{(2\cdot t_h/\Delta t_d)|k} \triangleq u_2, \\ &\ldots \\ u_{((n_h-1)\cdot t_h/\Delta t_d+1)|k} &= u_{((n_h-1)\cdot t_h/\Delta t_d+2)|k} = \ldots \\ &= u_{(n_h\cdot t_h/\Delta t_d)|k} \triangleq u_6. \end{aligned} \tag{34}$$

The sampling time Δt is set to 1 s, the adjustment parameter τ is 10, the particle quantity is 1000, and the maximum iteration number is 20. By solving the optimization problem (32) based on the latest measured state $x_{0|k}$ at each sampling instant, the optimal control sequence is obtained, and then the first element is applied to the system.

The controller and plant model are implemented together in dSPACE, wherein the run time of the plant model is negligible compared to that of the controller. The platform is shown in Fig. 16, and the real-time simulation results are shown in Fig. 17. The results reveal that the real-time control is realized under the hardware conditions. Fig. 17 shows that

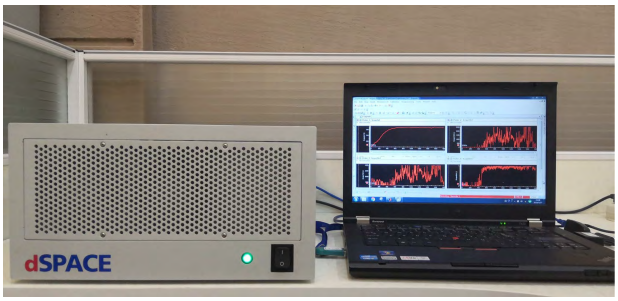

FIGURE 16. Platform for real-time simulations.

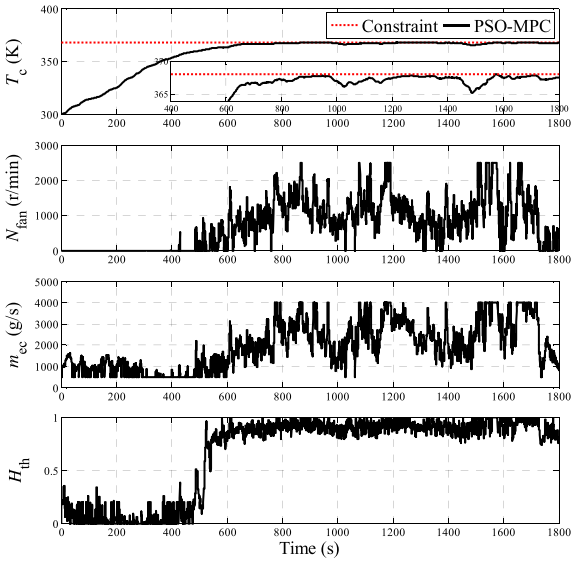

FIGURE 17. Results of the real-time implementation of the proposed control strategy using PSO-MPC with a limited horizon.

the state variable and control variables are basically consistent with those of the "Fuel-min optimal" controller except for some fluctuations in the control variables. The reason for these fluctuations is that the positions of the particles have a certain randomness, which is an inherent flaw of the PSO algorithm. The fuel consumption of the real-time simulation is 1808.74 g, which indicates the effectiveness and feasibility of the proposed strategy.

A knowledge of future driving conditions is a challenge for MPC application, however, for vehicles whose driving environment are certain or similar every day, e.g. taxis and buses, and vehicles equipped with a GPS combined with a traffic-flow information system, the Markov-based driving cycle generator can supply the driver's required vehicle speed to the controller, which is in a stochastic, average sense rather than a predetermined cycle [36], [37]. Moreover, with the development of V2V, V2I communications, advanced sensors, and automated vehicles, a knowledge of future driving conditions is possible to realize [38], [39].

VI. CONCLUSION

In this paper, a control strategy for minimum fuel consumption is proposed that accounts for both the engine friction caused by the coolant temperature and the actuator power of the cooling system. A physics-based dynamic heat transfer model of an electrified cooling system is developed. Two main intermediate variables—the heating power from the cylinder to the liner and the cooling power of the radiator—are focused on, and their characteristic variables are derived through an analysis of the heat transfer process, thereby, the accuracies of their fitting models are improved by at least 6.4% and 17.2%. To observe the effectiveness of the proposed strategy, a causal suboptimal controller using this strategy is compared with that for tracking the coolant temperature, which achieves 1.29%-2.76% fuel reduction under various driving cycles, and a DP-based optimal solution using this strategy is compared with that for minimizing the actuator power, which achieves 0.25%-0.46% fuel reduction, and this effect can increase as the environmental temperature decreases. Furthermore, this improvement has almost no cost. A comparison of the causal suboptimal solution and the DP-based optimal solution is also given to explore the potential of prediction, and the results show that a 0.27%-0.78% fuel reduction is achieved when the entire driving cycle is known. Moreover, the behavior of each controller is discussed and analyzed in detail according to the comparisons, which provides a basis for possible heuristic controllers in the future. Real-time implementation using PSO-MPC with a limited horizon is realized on a hardware platform, and the results indicates the feasibility and effectiveness of the proposed strategy.

REFERENCES

[1] Z. Dimitrova and F. Maréchal, "Energy integration on multi-periods and multi-usages for hybrid electric and thermal powertrains," *Energy*, vol. 83, pp. 539–550, Apr. 2015.
[2] I. Briggs, G. McCullough, S. Spence, and R. Douglas, "Whole-vehicle modelling of exhaust energy recovery on a diesel-electric hybrid bus," *Energy*, vol. 65, pp. 172–181, Feb. 2014.
[3] T. Alger, T. Chauvet, and Z. Dimitrova, "Synergies between high EGR operation and GDI systems," *SAE Int. J. Engines*, vol. 1, no. 1, pp. 101–114, 2009.
[4] T. Banjac, J. C. Wurzenberger, and T. Katrašnik, "Assessment of engine thermal management through advanced system engineering modeling," *Adv. Eng. Softw.*, vol. 71, pp. 19–33, May 2014.
[5] C. J. Brace, H. Burnham-Slipper, R. S. Wijetunge, N. D. Vaughan, K. Wright, and D. Blight, "Integrated cooling systems for passenger vehicles," SAE, Warrendale, PA, USA, Tech. Rep. 2001-01-1248, 2001.
[6] F. Melzer, U. Hesse, G. Rocklage, and M. Schmitt, "Thermomanagement," SAE, Warrendale, PA, USA, Tech. Rep. 1999-01-0238, 1999.
[7] D. J. Allen and M. P. Lasecki, "Thermal management evolution and controlled coolant flow," SAE, Warrendale, PA, USA, Tech. Rep. 2001-01-1732, 2001.
[8] F. Will and A. Boretti, "A new method to warm up lubricating oil to improve the fuel efficiency during cold start," *SAE Int. J. Engines*, vol. 4, no. 1, pp. 175–187 Dec. 2011.
[9] J. D. Trapy and P. Damiral, "An investigation of lubricating system warm-up for the improvement of cold start efficiency and emissions of S.I. automotive engines," SAE, Warrendale, PA, USA, Tech. Rep. 902089, 1990.
[10] M. Clough, "Precision cooling of a four valve per cylinder engine," SAE, Warrendale, PA, USA, Tech. Rep. 931123, 1993.
[11] A. Choukroun and M. Chanfreau, "Automatic control of electronic actuators for an optimized engine cooling thermal management," SAE, Warrendale, PA, USA, Tech. Rep. 2001-01-1758, 2001.
[12] K. B. Kim, K. W. Choi, K. H. Lee, and K. S. Lee, "Active coolant control strategies in automotive engines," *Int. J. Automot. Technol.*, vol. 11, no. 6, pp. 767–772, Dec. 2010.

[13] B. Zhou, X. Lan, X. Xu, and X. Liang, "Numerical model and control strategies for the advanced thermal management system of diesel engine," *Appl. Therm. Eng.*, vol. 82, pp. 368–379, May 2015.
[14] E. Cortona and C. H. Onder, "Engine thermal management with electric cooling pump," SAE, Warrendale, PA, USA, Tech. Rep. 2000-01-0965, 2000.
[15] R. Cipollone and D. Di Battista, "Sliding vane rotary pump in engine cooling system for automotive sector," *Appl. Therm. Eng.*, vol. 76, pp. 157–166, Feb. 2015.
[16] M. Bruckner, E. Gruenbacher, D. Alberer, L. del Re, and F. Atschreiter, "Predictive thermal management of combustion engines," in *Proc. Int. Conf. Control Appl.*, Munich, Germany, Oct. 2006, pp. 2778–2783.
[17] C. Vermillion, J. Sun, and K. Butts, "Modeling, control design, and experimental validation of an overactuated thermal management system for engine dynamometer applications," *IEEE Trans. Control Syst. Technol.*, vol. 17, no. 3, pp. 540–551, May 2009.
[18] F. Pizzonia, T. Castiglione, and S. Bova, "A robust model predictive control for efficient thermal management of internal combustion engines," *Appl. Energy*, vol. 169, pp. 555–566, May 2016.
[19] F. Caresana, M. Bilancia, and C. M. Bartolini, "Numerical method for assessing the potential of smart engine thermal management: Application to a medium-upper segment passenger car," *Appl. Therm. Eng.*, vol. 31, no. 16, pp. 3559–3568, Nov. 2011.
[20] M. H. Salah, T. H. Mitchell, J. R. Wagner, and D. M. Dawson, "Nonlinear-control strategy for advanced vehicle thermal-management systems," *IEEE Trans. Veh. Technol.*, vol. 57, no. 1, pp. 127–137, Jan. 2008.
[21] E. Bent, P. Shayler, A. La Rocca, and C. Rouaud, "The effectiveness of stop-start and thermal management measures to improve fuel economy," in *Proc. Vehicle Therm. Manage. Syst. Conf.*, Coventry, U.K., May 2013, pp. 27–39.
[22] J. R. Wagner, V. Srinivasan, D. M. Dawson, and E. E. Marotta, "Smart thermostat and coolant pump control for engine thermal management systems," SAE, Warrendale, PA, USA, Tech. Rep. 2003-01-0272, 2003.
[23] J. F. Eberth, J. R. Wagner, B. A. Afshar, and R. C. Foster, "Modeling and validation of automotive 'smart' thermal management system architectures," SAE, Warrendale, PA, USA, Tech. Rep. 2004-01-0048, 2004.
[24] C. Vermillion, J. Sun, and K. Butts, "Predictive control allocation for a thermal management system based on an inner loop reference model—Design, analysis, and experimental results," *IEEE Trans. Control Syst. Technol.*, vol. 19, no. 4, pp. 772–781, Jul. 2011.
[25] M. Nilsson, L. Johannesson, and M. Askerdal, "Assessing the potential of prediction in energy management for ancillaries in heavy-duty trucks," in *Proc. Eur. Control Conf.*, Strasbourg, France, Jun. 2014, pp. 1693–1698.
[26] *2005 ASHARE Handbook Fundamentals*, Amer. Soc. Heating Refrigerating Air-Conditioning Eng., Atlanta, GA, USA, 2005.
[27] M. Khodabakhshian, L. Feng, S. Börjesson, O. Lindgärde, and J. Wikander, "Reducing auxiliary energy consumption of heavy trucks by onboard prediction and real-time optimization," *Appl. Energy*, vol. 188, pp. 652–671, Feb. 2017.
[28] J. B. Heywood, *Internal Combustion Engine Fundamentals*. New York, NY, USA: McGraw-Hill, 1988.
[29] S. S. Bova, T. Castiglione, R. Piccione, and F. Pizzonia, "A dynamic nucleate-boiling model for CO_2 reduction in internal combustion engines," *Appl. Energy*, vol. 143, pp. 271–282 Apr. 2015.
[30] J. R. Wagner, E. E. Marotta, and I. Paradis, "Thermal modeling of engine components for temperature prediction and fluid flow regulation," SAE, Warrendale, PA, USA, Tech. Rep. 2001-01-1014, 2001.
[31] J. Lescot, A. Sciarretta, Y. Chamaillard, and A. Charlet, "On the integration of optimal energy management and thermal management of hybrid electric vehicles," in *Proc. IEEE Vehicle Power Propuls. Conf.*, Lille, France, Sep. 2010, pp. 1–6.
[32] S. M. Yang and W. Q. Tao, "Radiation heat transfer calculation," in *Heat Transfer*, 4th ed. Beijing, China: Higher Education Press, 2006, pp. 419–429.
[33] G. T. Chen and Y. Z. Wang, "Thermodynamic cycle," in *Engineering Thermodynamics*, 2nd ed. Beijing, China: Beijing Institute of Technology Press, 2008, pp. 192–206.
[34] A. P. Singh, S. Gadekar, and A. K. Agarwal, "In-cylinder air-flow characteristics using tomographic PIV at different engine speeds, intake air temperatures and intake valve deactivation in a single cylinder optical research engine," SAE, Warrendale, PA, USA, Tech. Rep. 2016-28-0001, 2016.
[35] F. Xu, H. Chen, X. Gong, and Q. Mei, "Fast nonlinear model predictive control on FPGA using particle swarm optimization," *IEEE Trans. Ind. Electron.*, vol. 63, no. 1, pp. 310–321, Jan. 2016.
[36] L. Johannesson, M. Asbogard, and B. Egardt, "Assessing the potential of predictive control for hybrid vehicle powertrains using stochastic dynamic programming," *IEEE Trans. Intell. Transp. Syst.*, vol. 8, no. 1, pp. 71–83, Mar. 2007.
[37] I. Kolmanovsky, I. Siverguina, and B. Lygoe, "Optimization of powertrain operating policy for feasibility assessment and calibration: Stochastic dynamic programming approach," in *Proc. Amer. Control Conf.*, Anchorage, AK, USA, May 2002, pp. 1425–1430.
[38] C. Sun, S. J. Moura, X. Hu, J. K. Hedrick, and F. Sun, "Dynamic traffic feedback data enabled energy management in plug-in hybrid electric vehicles," *IEEE Trans. Control Syst. Technol.*, vol. 23, no. 3, pp. 1075–1086, May 2015.
[39] C. M. Martinez, X. Hu, D. Cao, E. Velenis, B. Gao, and M. Wellers, "Energy management in plug-in hybrid electric vehicles: Recent progress and a connected vehicles perspective," *IEEE Trans. Veh. Technol.*, vol. 66, no. 6, pp. 4534–4549, Jun. 2017.

LIANG LU received the B.S. degree in thermal energy and power engineering from Jilin University, in 2013, where he is currently pursuing the Ph.D. degree in control theory and control engineering.

His research interests include modeling, optimal control, and nonlinear control for mechatronic systems, with an emphasis on their application to vehicular powertrain.

HONG CHEN received the B.S. and M.S. degrees in process control from Zhejiang University, Zhejiang, China, in 1983 and 1986, respectively, and the Ph.D. degree in system dynamics and control engineering from the University of Stuttgart, Stuttgart, Germany, in 1997. Since 1999, she has been a Professor with Jilin University, Changchun, China, where she currently serves as the Tang Aoqing Professor and as the Director of the State Key Laboratory of Automotive Simulation and Control. Her current research interests include model predictive control, optimal and robust control, and nonlinear control and applications in mechatronic systems focusing on automotive systems.

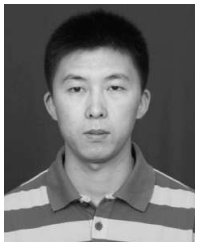

YUNFENG HU received the M.S. degree in basic mathematics and the Ph.D. degree in control theory and control engineering from Jilin University, Changchun, China, in 2008 and 2012, respectively.

He is currently an Associate Professor with the Department of Control Science and Engineering, Jilin University. His current research interests include nonlinear control and automotive control.

XUN GONG received the B.S. degree in electrical engineering from Northeast Electrical Power University, in 2010, and the Ph.D. degree in control theory and control engineering from Jilin University, in 2016.

He was a joint Ph.D. student and a Postdoctoral Researcher with the University of Michigan, Ann Arbor, MI, USA, from 2013 to 2015 and 2016 to 2018, respectively. His current research interests include model-based nonlinear control and optimal control, and control applications to automotive systems.

ZHIXIN ZHAO received the M.S. degree in basic mathematics from Yanbian University, China, in 2009, and the Ph.D. degree in systems engineering from the Beijing Institute of Information and Control, China.

He is currently an Associate Professor with the School of Mathematics, Changchun Normal University. His research focus is control in engineering.